AGU PUBLICATIONS

Geophysical Research Letters

RESEARCH LETTER
10.1002/2015GL066446

Key Points:
- Seismic anisotropy is ubiquitous throughout the Taiwan crust
- Crustal *S* wave splitting patterns correlate with arc collision tectonostratigraphic terranes
- Preferred mineral orientations cause *S* wave splitting in Taiwan metamorphic rocks

Supporting Information:
- Text S1
- Table S1

Correspondence to:
D. Okaya,
okaya@usc.edu

Citation:
Okaya, D., N. I. Christensen, Z. E. Ross, and F. T. Wu (2016), Terrane-controlled crustal shear wave splitting in Taiwan, *Geophys. Res. Lett.*, *43*, 556–563, doi:10.1002/2015GL066446.

Received 6 OCT 2015
Accepted 17 DEC 2015
Accepted article online 19 DEC 2015
Published online 16 JAN 2016

Terrane-controlled crustal shear wave splitting in Taiwan

David Okaya[1], Nikolas I. Christensen[2], Zachary E. Ross[1], and Francis T. Wu[3]

[1]Department Earth Sciences, University of Southern California, Los Angeles, California, USA, [2]Earth, Ocean, and Atmospheric Sciences, University of British Columbia, Vancouver, British Columbia, Canada, [3]Department Geological Sciences, SUNY/Binghamton, Binghamton, New York, USA

Abstract Taiwan is the result of arc-continent collision associated with the convergence of the Philippine Sea plate with the eastern Eurasian plate continental margin. The locus of deformation is found in eastern Taiwan in the form of mountain building (Central Range) with underlying thickened lithosphere. Rapid tectonic exhumation in the Central Range has uncovered low-to-high-grade metamorphic rocks marked by steep cleavage. We carried out a crustal seismic anisotropy study across Taiwan, producing a database of over 27,000 local earthquake shear wave splitting measurements. Additionally, we carried out rock physics measurements of metamorphic outcrop samples to quantify shear wave rock anisotropy. We produced a map of station-averaged splitting measurements across Taiwan. Patterns of fast shear wave directions correlate with tectonic terranes produced by plate convergence. Deformation-related mineral-preferred orientation in the metamorphic rocks produces a significant amount of the crustal anisotropy in the Taiwan collision zone.

1. Introduction

Crustal seismic anisotropy has been observed within many orogenic belts and active plate boundaries and is the result of tectonic activity within the crust. This type of anisotropy can be caused by two major changes due to deformation. First, fracture fields that have developed due to regional or local stress will have faster seismic velocities oriented parallel to the fractures. These fractures may be pervasive in the zone of deformation, particularly adjacent to fault zones or within plate boundary orogens. These fractures, however, will commonly close with depth due to increasing confining pressure and metamorphic reactions. Second, rock fabrics due to deformation-related shearing or metamorphism can produce strong crustal seismic anisotropy due to alignment of minerals which themselves are seismically anisotropic. Minerals in continental crust primarily responsible for seismic anisotropy include phyllosilicates and amphiboles [e.g., *Christensen*, 1965, 1966; *Godfrey et al*., 2000]. Fabric-related anisotropy can be produced at all crustal levels and be regionally pervasive or have its own three-dimensional configuration.

Taiwan is the product of oblique arc-continent collision at the Eurasian-Philippine Sea plate boundary. This ongoing convergence (~80 mm/yr) produces a rapidly exhuming mountain range that exhibits near-vertical fabrics (regional cleavage and foliation) due to transpression. Several recent studies have identified crustal seismic anisotropy across Taiwan due to stress-induced fractures and material fabrics associated with this convergence. Regional stress anisotropy has been inferred using local shear wave splitting [*Liu et al*., 2004; *Tai et al*., 2011], surface waves [*Lai et al*., 2009], and teleseismic shear waves [*Huang et al*., 2006; *Kuo-Chen et al*., 2009]. Vertical coherence of mantle and crustal deformation have been interpreted by *Rau et al*. [2000] using teleseismic shear waves and by *Kuo-Chen et al*. [2013] using regional earthquake *P* waves. *Chang et al*. [2009] used shear wave splitting to identify anisotropy that is orogen-parallel (N-S) in eastern Taiwan but orogen-perpendicular (E-W) in western Taiwan (e.g., fabric versus stress fractures, respectively). In contrast, *Huang et al*. [2015] used ambient noise surface waves to interpret the Taiwan upper crust as orogen-parallel (collision-related) and the lower crust as orogen-perpendicular (plate convergence-related).

The U.S.-Taiwan collaborative project "Taiwan Integrated Geodynamics Research" (TAIGER) examined 3-D geodynamical concepts of this arc collision and mountain building. In order to obtain observational constraints, this project carried out geophysical experiments across and surrounding Taiwan during 2005–2009 [e.g., *Wu et al*., 2014] including active-source seismic onshore-offshore profiling [*Van Avendonk et al*., 2014]. In this paper, we present the results of a body wave shear wave splitting study across Taiwan using earthquakes found in

the continuous data collected during the TAIGER seismic onshore-offshore profiling experiment in 2009. Specifically, we used only well-located local earthquakes whose wave paths were limited to within the crust (i.e., no mantle contamination). This experiment used seven linear transects for a total of 279 stations at 2 to 5 km spacings; these data provide higher spatial resolution compared to other earlier efforts. As a result, our shear wave splitting results illustrate regional patterns and internal heterogeneity that we interpret to correlate with Taiwan's terranes. Combining with our rock physics studies of Central Range metamorphic rocks, we explore direct links between rock fabrics and observable seismic anisotropy.

2. Taiwan Terranes

The island of Taiwan is forming as the Luzon arc, at the leading edge of the Philippine Sea plate (moving N50°W at ~80 mm/yr), obliquely collides with the continental margin of the Eurasian plate. The dominant expressions of the deformation and shortening associated with this collision are (1) the Central Range, a NNE-SSW oriented mountain range on the eastern side of the island created by collision-related exhumation, and (2) a fold and thrust belt in western Taiwan that is essentially being pushed by the collision zone from the east [*Wu et al*., 2014].

There are seven distinct physiographic and tectonostratigraphic terranes in Taiwan (Figure 1b) described here from west to east. The Coastal Plain (CP) is a set of foreland subbasins with 3–12 km surface alluvium and Neogene strata overlying Eurasian plate basement [*Huang et al*., 2013]. The Western Foothills (WF) contains a west vergent fold and thrust belt of Tertiary clastic sedimentary rocks separated from the underlying Eurasian basement by a regional low-angle décollement [e.g., *Suppe*, 1980]. Maximum compressive stress here is subhorizontal and trends WNW-ESE approximately parallel with the convergence direction of the Philippine Sea plate [*Angelier et al*., 1986]. The Hsuehshan Range (HR), slate belt (SB), and metamorphic belt (MM) are NNE-SSW belts that represent different structural elements within the deformation caused by arc collision. The HR consists of thick sequences of early Tertiary folded metasandstones, slates, and phyllites. The SB and MM compose the Central Range. The SB is predominantly mid-Tertiary slates and phyllites, whereas the MM contains higher-grade gneisses, marbles, and schists of older Eurasian provenance. Of importance are well-developed regional cleavage patterns across these terranes. Cleavage strike is terrane-parallel and is subparallel to the terrane boundaries (Figure 1). Originally thought to fan across the range, the weakly developed east dipping cleavage in HR becomes more intense and steeply dipping in SB [e.g., *Clark and Fisher*, 1995]. In contrast, the MM cleavage is steeply west dipping, and the boundary between these dip domains is still in debate [*Fisher et al*., 2007; *Brown et al*., 2012]. Cleavage development is associated with rapid exhumation of these terranes (4–10 mm/yr [*Lee et al*., 2006]) from midcrustal depths [*Fisher et al*., 2007]. The structural distribution and geometries of these belts at mid-to-lower crustal levels are not clearly resolved [e.g., *Wu et al*., 2014]. The Coastal Range (CR) is the northern extension of the Luzon volcanic arc and fore-arc basin that has collided with and accreted to Taiwan. This terrane consists of dominantly andesitic arc rocks with associated volcanoclastics [*Ho*, 1986]. An oblique thrust dipping under southern CR defines the suture with the Central Range orogen [*Lee et al*., 2006]. The Longitudinal Valley (LV) is a deep alluvial basin generally regarded as the collisional suture [e.g., *Lewis et al*., 2015].

3. TAIGER Seismological Data

The original purpose of the seismic onshore-offshore survey was to collect marine air gun sources provided by the R/V *Langseth* into continuously recording land-based portable instruments and ocean bottom seismometers. The high seismicity rate across Taiwan presented the opportunity to create the unique and independent data set of earthquakes extracted from an active-source seismic data volume. The original land-based seismic onshore-offshore instruments were arranged into a grid of linear arrays in order to carry out high-resolution travel time tomography and waveform imaging along 2-D transects [e.g., *van Avendonk et al*., 2014] and combined passive/active-source 3-D regional tomography [*Wu et al*., 2014]. Instrumentation for 279 stations was provided by Incorporated Research Institutions for Seismology (IRIS) Program for Array Seismic Studies of the Continental Lithosphere and Taiwan academic institutions. Sensors were predominantly short period with locally interspersed intermediate period. The four east-west arrays (T4A–T6 in Figure 1a) used nominal 2 km station spacing and a recording period of 2.5 months. The three north-south arrays (T7–T9) used nominal 5 km spacing during up to 6 month recording.

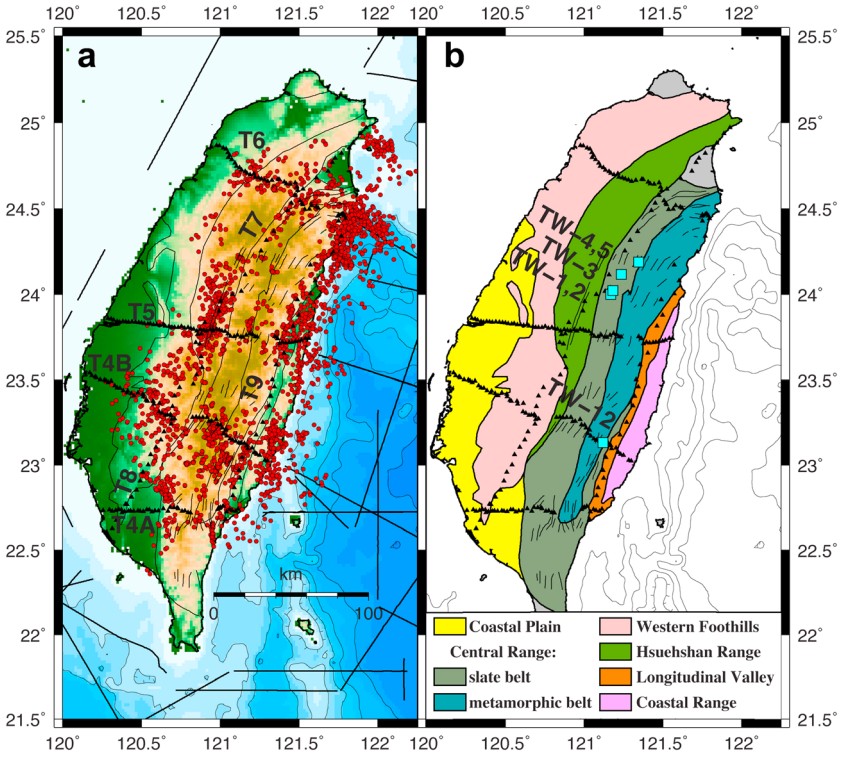

Figure 1. Location of Taiwan seismological data used in this study. (a) TAIGER seismic onshore-offshore experiment included 279 land stations (black triangles) plus marine air gun tracks (lines). Seismicity (red circles) is collected during onshore-offshore experiment that produced shear wave splitting, original detection and relocations by F. T. Wu et al., submitted manuscript (2015). (b) Geological terranes. Central Range is composed primarily of metamorphic rocks. Light grey is Qal basins. Strike of metamorphic fabrics (short black lines). Locations of outcrop samples for petrophysics acoustic measurements (cyan squares).

4. Shear Wave Splitting Analysis

The shear wave splitting study reported here was performed in two major steps: (1) detection and location of local earthquakes that occurred during the 2009 TAIGER seismic onshore-offshore survey and extraction of a waveform data set, followed by (2) passing the local earthquake shear waves through shear wave splitting analysis software designed to handle significantly large volumes of data.

A catalogue of local earthquakes contained in this data volume was produced by F. T. Wu et al., Dense network, intense seismicity, and tectonics of Taiwan, submitted to *Tectonophysics* (2015) using statistics-based *P* and *S* wave detection and picking methods [*Ross and Ben-Zion*, 2014a, 2014b] and relocation of initial locations using the HypoDD method [*Waldhauser and Ellsworth*, 2000]. This new catalogue has 4863 local earthquakes (Figure 1a), an increase of 46% more than the national Central Weather Bureau official catalogue for the same time period, particularly in the magnitude 1 to 2.5 range [F. T. Wu et al., submitted manuscript, 2015].

The shear wave splitting analysis used the Multiple Filter Automatic Splitting Technique (MFAST) software package developed by Victoria University of Wellington [*Savage et al.*, 2010; *Wessel et al.*, 2013]. This package was designed to automate the processing of large numbers of source-to-station shear waves in order to obtain many splitting parameters of delay times and fast shear wave directions (δt and ϕ, respectively). The package wraps the splitting method of *Silver and Chan* [1991] with a cluster analysis method of *Teanby et al.* [2004] and carries out the splitting calculations using a self-determined optimal frequency filter bandwidth per individual shear wave. In addition, MFAST assigns a quality grade (A–D) to each set of splitting parameters based on factors such as cluster analysis and signal-to-noise ratio.

Bulk MFAST processing of our earthquakes into portions of the 279 stations yielded 42,155 individual source-station pairs of splitting parameters (grades A–D). Of these, 27,780 were of grade A (highest). We subsequently winnowed these results based on source-station geometry in order to restrict wave paths

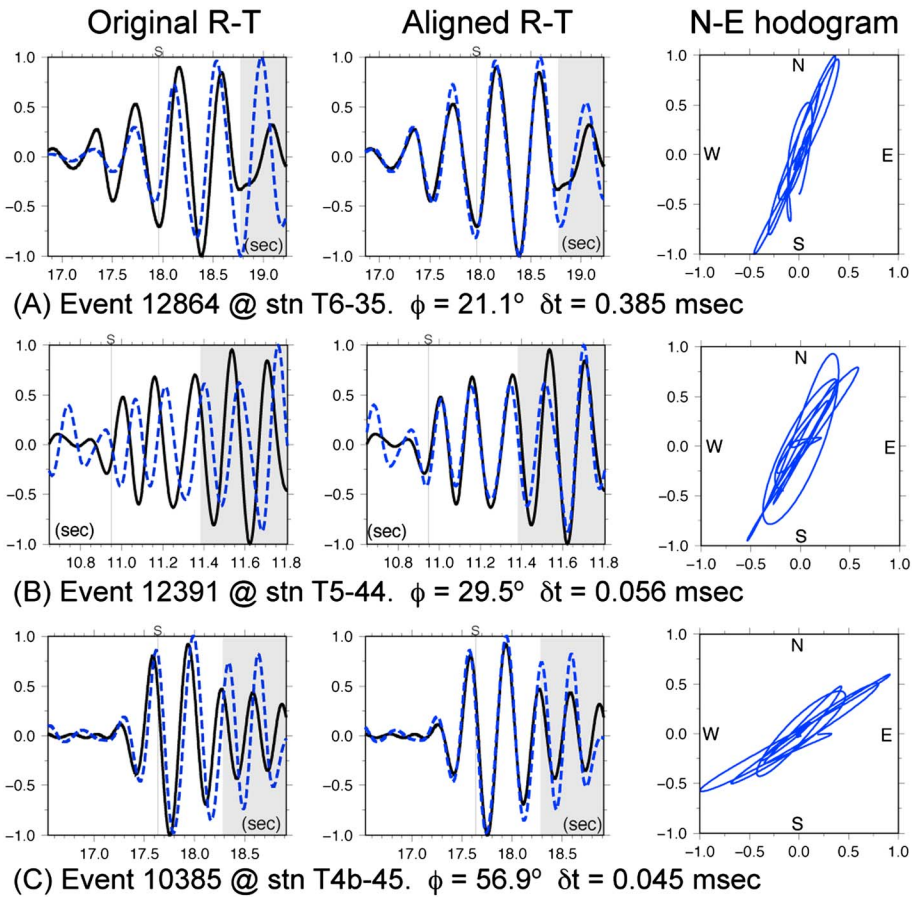

Figure 2. Examples of highest-quality shear wave splitting analysis using MFAST splitting package [*Savage et al.*, 2010]. Shear waves are shown for individual events at stations on three different transects. (left column) Original scaled radial (solid) and transverse (dashed) components and (middle column) after alignment for splitting time. (right column) Hodograms of corrected shear wave particle motion.

to within the Taiwan crust; sources were limited to 30 km depth and epicentral path lengths to less than 60 km which is short of the upper mantle *Pn* refraction crossover distance [*van Avendonk et al.*, 2014]. This produced a database of grade A shear wave splitting parameters for 21,068 source-station combinations. These measurements are distributed across Taiwan at a wide range of back azimuths and inclination angles based on propagation directions. Figure 2 illustrates highest-quality measurements using plots generated by MFAST for stations located within the slate belt.

In order to search for regional patterns of crustal anisotropy, we reduced the large number of winnowed splitting parameters by averaging the fast directions and splitting times at each station. The average fast directions were calculated using a circular averaging method, splitting times reduced via arithmetic means, and the uncertainties via root-mean-square averaging. A table is provided as online Supporting Information of the resulting δt-ϕ averages for all (253) stations that possess grade A measurements. A map of the station-averaged splitting measurements is shown in Figure 3; we interpret the patterns in section 6.

5. *S* Wave Velocities and Splitting in Central Range Rocks

Laboratory studies of shear wave propagation in crustal rocks of the types found in the Central Range have shown that slates and their higher-grade equivalents, phyllites and mica schists, exhibit the highest anisotropies of common metamorphic rocks [*Christensen*, 1965, 1966; *Godfrey et al.*, 2000; *Christensen and Okaya*, 2007; *Bostock and Christensen*, 2012]. These studies have provided important information on the magnitude, symmetry, and origin of *S* wave splitting in low- and medium-grade metamorphic terranes containing metapelites. In this study we collected rock samples in the Central Range and obtained *S* wave velocity

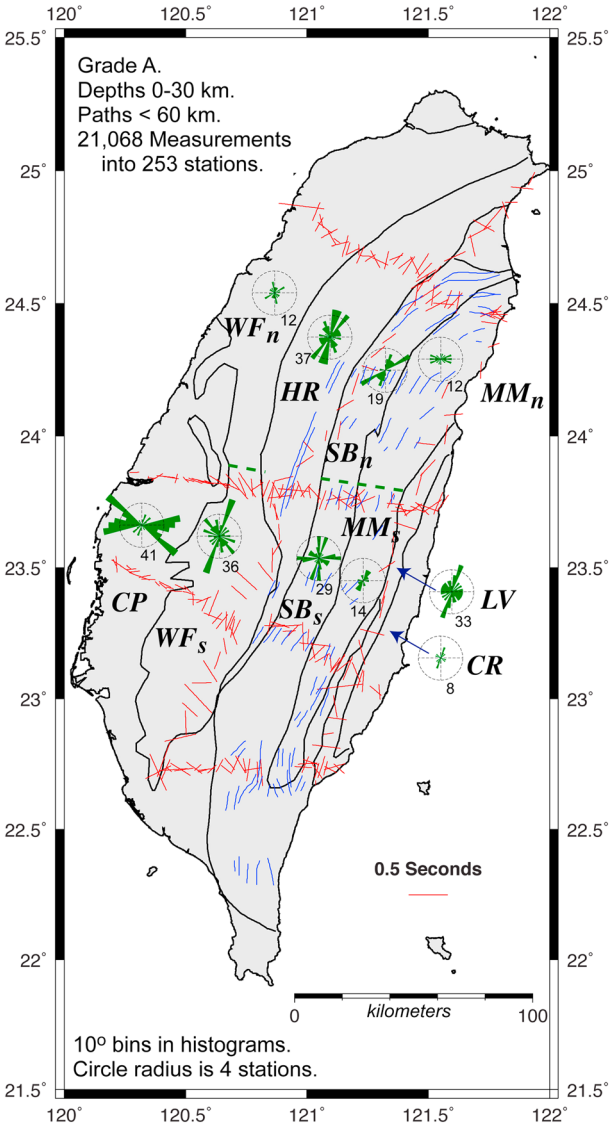

Figure 3. Crustal shear wave splitting patterns across Taiwan. Red bars are the station-averaged shear wave splitting results. Individual splitting measurements are produced using MFAST prior to averaging. Polar histograms indicate azimuthal distribution of fast splitting directions (10° bin width). For each histogram, circle radius is four stations; number at bottom is the total number of stations. Green dashed line indicates the boundary for northern and southern histograms for WF, SB, and MM; see text. Blue bars indicate the trends of rock fabrics in SB and MM belts. Geological terranes are identified in Figure 1.

measurements to hydrostatic pressures of 1000 MPa (~35 km depth), with subsequent calculations of direction-dependent velocities for four highly anisotropic slates in the SB and a quartz-mica schist from MM. In addition, *S* wave velocities were measured for an isotropic metagreywacke. Sample localities are shown in Figure 1b. The slates have well-developed cleavage resulting from strong alignment of platy phyllosilicates. All the rocks are fine-grained and compositionally homogeneous, qualities ideal for laboratory-scale measurements.

The velocities were measured from 2.54 cm diameter cores using a pressure vessel and the pulse transmission technique described by *Christensen* [1985]. Lead zirconate titanate transducers with resonant frequencies of 1 MHz generated and received the *S* waves. Velocity measurements using this technique are believed to be accurate to within 1%. Bulk densities were calculated from the weights and volumes of the measured cores.

Based on thin section and hand sample analyses, the symmetries of the slates and the schist are to a first approximation transversely isotropic (TI; hexagonal symmetry), with symmetry axes normal to their cleavage or foliation. One sample (TW-5) shows some variability in velocities for propagation within the cleavage plane that contains a pronounced lineation and thus in a strict sense is likely orthorhombic. *S* wave velocities of the slates and schist are presented in Table 1 as a function of confining pressure for propagation perpendicular and parallel to the cleavage, the latter direction which usually shows the maximum splitting [e.g., *Christensen*, 1966; *Godfrey et al*., 2000]. *VSh* is velocity of the *S* wave vibrating in the plane of the cleavage, and *VSv* is for the *S* wave vibrating parallel to the symmetry axis. All velocities are for pure modes. Anisotropies expressed as a percentage of the mean velocity are significantly large for the slates (Table 1) and are directly related to mineral alignment.

Calculated *S* wave velocity curves as a function of seismic propagation angle to the cleavage or foliation normals are shown in Figure 4 for the rock samples, whose equations are summarized in *Johnston and Christensen* [1995] and *Okaya and Christensen* [2002], among others. Velocities in Figure 4 are shown at 400 MPa, a pressure well above the closing pressure of microcracks. Two features in these curves are notable. First, unlike for pure elliptical TI material where *qSh* is faster than *qSv* for all nonaxial directions, the shear wave velocities in these slates and schist samples exhibit "crossover," where *qSv* is the faster velocity for

Table 1. Rock Physics Laboratory Measurements for Five Anisotropic Samples (Four Slate and One Schist) and One Isotropic Sample (Greywacke)[a]

						Pressure (MPa)					
Sample	Phase	20	40	60	80	100	200	400	600	800	1000
TW-1	$\rho = 2742$										
Slate	VSv	2.653	2.712	2.749	2.777	2.800	2.876	2.962	3.017	3.059	3.093
121.1689°E	VSh	3.533	3.561	3.579	3.593	3.605	3.646	3.696	3.730	3.757	3.780
24.0009°N	%VS	28%	27%	26%	26%	25%	24%	22%	21%	20%	20%
TW-2	$\rho = 2652$										
Slate	VSv	2.370	2.474	2.539	2.588	2.627	2.759	2.899	2.979	3.032	3.070
121.1819°	VSh	3.665	3.715	3.745	3.767	3.785	3.842	3.904	3.941	3.969	3.991
24.0228°	%VS	43%	40%	38%	37%	36%	33%	30%	28%	27%	26%
TW-4	$\rho = 2699$										
Slate	VSv	2.832	2.947	3.012	3.057	3.092	3.196	3.298	3.357	3.398	3.429
121.3463°	VSh	3.864	3.892	3.909	3.921	3.931	3.962	3.995	4.016	4.033	4.046
24.1899°	%VS	31%	28%	26%	25%	24%	21%	19%	18%	17%	17%
TW-5	$\rho = 2712$										
Slate	VSv	2.970	2.765	3.107	3.140	2.903	2.992	3.074	3.120	3.152	3.176
121.3463°	VSh	3.980	4.032	4.059	4.077	4.091	4.129	4.163	4.180	4.192	4.201
24.1899°	%VS	29%	37%	27%	26%	34%	32%	30%	29%	28%	28%
TW-12	$\rho = 2589$										
Schist	VSv	2.993	3.163	3.252	3.310	3.352	3.471	3.575	3.630	3.666	3.693
121.1201°	VSh	3.499	3.653	3.727	3.773	3.806	3.893	3.962	3.995	4.017	4.032
23.1334°	%VS	16%	14%	14%	13%	13%	11%	10%	10%	9%	9%
TW-3	$\rho = 2627$										
Greywacke	Vs	2.970	2.765	3.107	3.140	2.903	2.992	3.074	3.120	3.152	3.176
121.2371°											
24.1182°											

[a]Shear wave velocities in km/s and densities (ρ) in kg/m^3. $\%VS = (VSh - VSv)/\{0.5 \times (VSh + VSv)\}$. Sample locations are shown in Figure 1; longitude-latitude is listed beneath rock type of each sample.

directions closer to the symmetry axis and *qSh* is faster in directions near the cleavage planes. Thus, within the same rock, a 90° switch in fast *S* direction, ϕ, occurs at this crossover. Second, because the velocity crossovers are in the 40–55° directions, the maximum detectable shear wave splitting is limited to ~60–90° propagation directions. For vertical cleavage in the Central Range the optimal directions for shear wave splitting paths are thus parallel to strike or in the near-vertical dip direction.

6. Discussion and Conclusions

The patterns of station-averaged shear wave fast vibration directions (splitting bars) shown in Figure 3 change across the island and correlate with the terranes. Individual station-to-station variations exist for reasons including these factors: (a) local heterogeneity in near-surface geology or seismic stations, (b) the large number of individual splitting measurements being averaged (up to 370; Supporting Information), (c) the wide range of back azimuth and inclination raypath angles in the individual measurements, and (d) possibly the shear wave velocity crossover effect in the Central Range rocks.

In Figure 3 we include polar histograms that summarize the statistical patterns within and across terranes. Due to along-strike changes in the WF, SB, and MM terranes, those splitting results are subdivided into northern and southern histograms. The entirety of CP is primarily in the south and HR within the north. Shear wave fast directions in the CP are narrowly bimodal in the E-W and WNW-ESE directions. In the adjacent southern WF the fast directions are in transition to NW-SE to NNE-SSW. The fast directions in northern WF and HR are dominantly NNE. Within the full SB and MM, the fast directions correlate with the slate cleavage strikes, with both showing an overall NNE direction but with internal second-order lateral undulations. In addition, the fast directions and cleavage strikes take a sharp eastward turn in the northernmost MM, mimicking the geology strikes. The LV and CR fast directions are also NNE-oriented, parallel to the long axes of the valley and arc terranes.

The interpretation of the shear wave splitting is tied to the arc collision tectonics due to the NW convergent Philippine Sea plate. While deformation is maximal in the Central Range, it reaches westward as expressed as the WF foreland fold and thrusts. We interpret in the CP, further west of this deformation, the shear wave

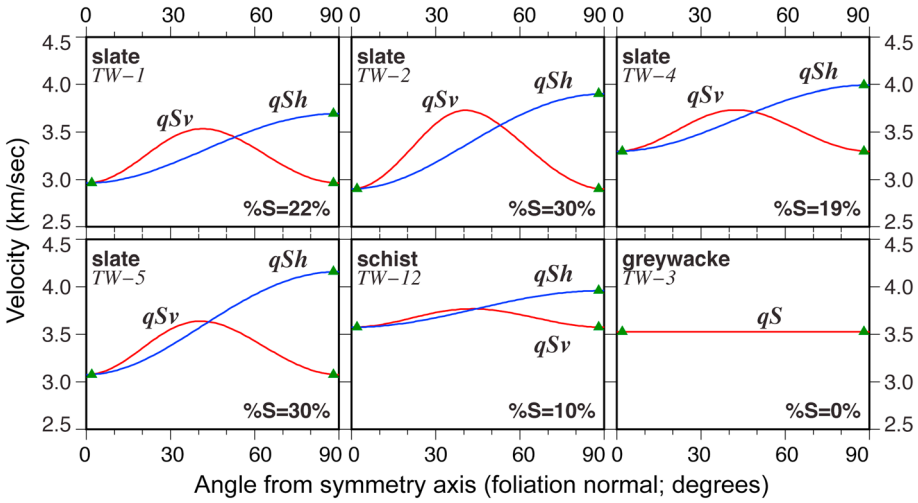

Figure 4. Laboratory measurements of *S* wave velocities at 400 MPa confining pressure (green triangles) and calculated velocities at propagation angles to the foliation normals. Sample locations are given in Figure 1. Blue curves are the velocities for *S* waves vibrating parallel to the foliation/cleavage planes. Note that for propagation subparallel to foliation normal, fast *S* no longer vibrates parallel to the foliation (red curves at angles less than crossover angle; see text).

splitting to be due to upper crustal regional stress cracks consistent with *Chang et al*. [2003] or rock anisotropy in the Eurasian basement. The primary features in the northern WF are the fold and thrust structures; the fast directions are aligned with the overall strike of the fold axes. The southern WF is similar but includes the transition from the CP. We suggest that the steeply dipping cleavage domains in the eastern HR, SB, and MM are primarily responsible for the NNE-SSW splitting directions and regional along-strike variations. Strong SB anisotropy is consistent with its slate belt geology (near-vertical cleavage [*Tillman and Byrne*, 1995; *Fisher et al*., 2007]). A majority of the fast vibration directions are parallel to strikes of the slaty cleavage. Observations of E-W splitting in the southern SB could result from propagation perpendicular to the N-S striking cleavage (e.g., the *qSv/qSh* reversal in what is "fast VS" in Figure 4) or from the presence of lower symmetry rocks. The LV is generally regarded as the arc-continent suture zone whose shear can produce anisotropic mylonite zones that are shear zone parallel. If steeply dipping, this zone can produce the valley-parallel patterns [e.g., *Lewis et al*., 2015]. Since arc rocks such as those found in the CR are primarily isotropic [e.g., *Miller and Christensen*, 1994], the observed splitting may be due to shear zones related to and subparallel to the collision zone. In addition, *Shyu et al*. [2006] suggested that a sliver of fore-arc crust underlies this region due to the arc collision. Thus, metamorphosed accretionary sediments could also contribute to the CP splitting observations.

We conclude that the shear wave splitting patterns within the terranes are related to the tectonic deformation caused during arc collision. The strong horizontal convergence and vertical exhumation within the Central Range accentuates inherent anisotropy in low-grade cleavage and higher-grade metamorphic foliation due to internal mineral preferred orientations. Further exploration of our large database of anisotropy results may reveal that vertical and even material symmetry heterogeneity exist and that advanced anisotropy methods should be applied to better understand both compressional and shear wave anisotropies of Taiwan's terranes.

Acknowledgments
This study was funded by the NSF Continental Dynamics program under awards NSF EAR-1009691 (D.O.), EAR-0410227 (N.C.), and EAR-1010645 (F.W.). We thank Martha Savage and an anonymous reviewer for their helpful comments. We also thank Wen-Tzong Liang, C.-Y. Wang, and B.-S. Huang for providing additional seismological data and Yuan-Hsi Lee who guided our field excursion to collect Central Range rock samples. Seismological waveform data used in this study are available from the Taiwan TEC Data Center (http://www.tecdc.earth.sinica.edu.tw) and from IRIS DMC (http://www.iris.edu). The authors created the figures using GMT [*Wessel and Smith*, 2013].

References

Angelier, J., E. Barrier, and H. T. Chu (1986), Plate collision and paleostress trajectories in a fold and thrust belt: The foothills of Taiwan, *Tectonophysics*, *125*, 161–178.

Bostock, M. G., and N. I. Christensen (2012), Split from slip and schist: Crustal anisotropy beneath northern Cascadia from non-volcanic tremor, *J. Geophys. Res.*, *117*, B08303, doi:10.1029/2011JB009095.

Brown, D., J. Alvarez-Marron, M. Schimmel, Y.-M. Wu, and G. Camanni (2012), The structure and kinematics of the central Taiwan mountain belt derived from geological and seismicity data, *Tectonics*, *31*, TC5013, doi:10.1029/2012TC003156.

Chang, C.-P., T.-Y. Chang, J. Angelier, H. Kao, J.-C. Lee, and S.-B. Yu (2003), Strain and stress field in Taiwan oblique convergent system: Constraints from GPS observation and tectonic data, *Earth Planet. Sci. Lett.*, *214*, 115–127.

Chang, E. T. Y., W.-T. Liang, and Y.-B. Tsai (2009), Seismic shear wave splitting in upper crust characterized by Taiwan tectonic convergence, *Geophys. J. Int.*, *177*, 1256–1264.

Christensen, N. I. (1965), Compressional wave velocities in metamorphic rocks at pressures to 10 kilobars, *J. Geophys. Res.*, *70*, 6147–6164.
Christensen, N. I. (1966), Shear wave velocities in metamorphic rocks at pressures to 10 kilobars, *J. Geophys. Res.*, *71*, 3549–3556.
Christensen, N. I. (1985), Measurements of dynamic properties of rock at elevated temperatures and pressures, in *Measurement of Rock Properties at Elevated Pressures and Temperatures*, edited by H. J. Pincus and E. R. Hoskins, pp. 93–107, American Society for Testing and Materials, Philadelphia, Pa.
Christensen, N. I., and D. Okaya (2007), Compressional and shear wave velocities in South Island NZ rocks and their application to the interpretation of seismological models of the New Zealand crust, in *A Continental Plate Boundary: Tectonics of South Island, New Zealand*, *AGU Geophys. Monogr.*, vol. 175, edited by D. Okaya, T. Stern, and F. Davey, pp. 125–158, AGU, Washington, D. C.
Clark, M. B., and D. M. Fisher (1995), Strain partitioning and crack-seal growth of chlorite-muscovite aggregates during progressive non-coaxial strain: An example from the slate belt of Taiwan, *J. Struct. Geol.*, *17*, 461–474.
Fisher, D. M., S. Willet, E.-C. Yeh, and M. B. Clark (2007), Cleavage fronts and fans as reflections of orogen stress and kinematics in Taiwan, *Geology*, *35*, 65–68, doi:10.1130/G22850A.1.
Godfrey, N. J., N. I. Christensen, and D. A. Okaya (2000), Anisotropy of schists: Contributions of crustal anisotropy to active-source seismic experiments and shear-wave splitting observations, *J. Geophys. Res.*, *105*, 27,991–28,007, doi:10.1029/2000JB900286.
Ho, C. S. (1986), A synthesis of the geologic evolution of Taiwan, *Tectonophysics*, *125*, 1–16.
Huang, B.-S., W.-G. Huang, W.-T. Liang, R.-J. Rau, and N. Hirata (2006), Anisotropy beneath an active collision orogen of Taiwan: Results from across islands array observations, *Geophys. Res. Lett.*, *33*, L24302, doi:10.1029/2006GL027844.
Huang, B.-S., C.-Y. Chien, D. Okaya, S.-J. Lee, Y.-C. Lai, F. T. Wu, W.-T. Liang, and W.-G. Huang (2013), Multiple diving waves and high-velocity gradients in the western Taiwan Coastal Plain—An investigation based on the TAIGER experiment, *Bull. Seismol. Soc. Am.*, *103*, 925–935, doi:10.1785/0120110047.
Huang, T.-Y., Y. Gung, B.-Y. Kuo, L.-Y. Chiao, and Y.-N. Chen (2015), Layered deformation in the Taiwan orogen, *Science*, *349*, 720–723, doi:10.1126/science.aab1879.
Johnston, J., and N. Christensen (1995), Seismic anisotropy of shales, *J. Geophys. Res.*, *100*, 5991–6003.
Kuo-Chen, H., F. T. Wu, D. Okaya, B.-S. Huang, and W.-T. Liang (2009), SKS/SKKS splitting and Taiwan orogeny, *Geophys. Res. Lett.*, *36*, L12303, doi:10.1029/2009GL038148.
Kuo-Chen, H., P. Sroda, F. Wu, C.-Y. Wang, and Y.-W. Kuo (2013), Seismic anisotropy of the upper crust in the mountain ranges of Taiwan from the TAIGER explosion experiment, *Terr. Atmos. Ocean Sci.*, *24*, 963–970, doi:10.3319/TAO.2013.07.30.01(T).
Lai, Y.-C., B.-S. Huang, and H.-Y. Yen (2009), Azimuthal anisotropy beneath the Central Taiwan from array analysis of fundamental-mode Rayleigh waves, Eos Trans. AGU, 90(52), Fall Meet. Suppl., Abstract T33B-1906.
Lee, Y.-H., C.-C. Chen, T.-K. Liu, H.-C. Ho, H.-Y. Lu, and W. Lo (2006), Mountain building mechanisms in the southern Central Range of the Taiwan orogenic belt—From accretionary wedge deformation to arc-continental collision, *Earth Planet. Sci. Lett.*, *252*, 413–422.
Lewis, J. C., D. J. O'Hara, and R.-J. Rau (2015), Seismogenic strain across the transition from fore-arc slivering to collision in southern Taiwan, *J. Geophys. Res. Solid Earth*, *120*, 4539–4555, doi:10.1002/2015JB011906.
Liu, Y., T.-L. Teng, and Y. Ben-Zion (2004), Systematic analysis of shear-wave splitting in the aftershock zone of the 1999 Chi-Chi, Taiwan, earthquake: Shallow crustal anisotropy and lack of precursory variations, *Bull. Seismol. Soc. Am.*, *94*, 2330–2347, doi:10.1785/0120030139.
Miller, D. J., and N. I. Christensen (1994), Seismic signature and geochemistry of an island arc: A multidisciplinary study of the Kohistan accreted terrane, northern Pakistan, *J. Geophys. Res.*, *99*, 11, 623–11, 642.
Okaya, D., and N. I. Christensen (2002), Anisotropic effects of non-axial seismic wave propagation in foliated crustal rocks, *Geophys. Res. Letts.*, *29*(11), 1507, doi:10.1029/2001GL014285.
Rau, R.-J., W.-T. Liang, H. Kao, and B.-S. Huang (2000), Shear wave anisotropy beneath the Taiwan orogen, *Earth Planet. Sci. Lett.*, *177*, 177–192.
Ross, Z. E., and Y. Ben-Zion (2014a), An earthquake detection algorithm with pseudo probabilities of multiple indicators, *Geophys. J. Int.*, *197*, 458–463, doi:10.1093/gji/ggt516.
Ross, Z. E., and Y. Ben-Zion (2014b), Automatic picking of direct *P*, *S* seismic phases and fault zone head waves, *Geophys. J. Int.*, *199*, 368–381, doi:10.1093/gji/ggu267.
Savage, M. K., A. Wessel, N. Teanby, and T. Hurst (2010), Automatic measurement of shear wave splitting and applications to time varying anisotropy at Mt. Ruapehu volcano, New Zealand, *J. Geophys. Res.*, *115*, B12321, doi:10.1029/2010JB007722.
Shyu, J. H., K. Sieh, Y.-G. Chen, and L.-H. Chung (2006), Geomorphic analysis of the Central Range fault, the second major active structure of the Longitudinal Valley suture, eastern Taiwan, *Geol. Soc. Am. Bull.*, *118*, 1447–1462, doi:10.1130/B25905.1.
Silver, P. G., and W. W. Chan (1991), Shear wave splitting and subcontinental mantle deformation, *J. Geophys. Res.*, *96*, 16,429–16,454.
Suppe, J. (1980), Imbricated structure of western foothills belt, south-central Taiwan, *Pet. Geol. Taiwan*, *17*, 1–16.
Tai, L.-X., Y. Gao, K.-F. Ma, E.-T. Lee, Y.-T. Shi, and H.-I. Lin (2011), Crustal anisotropy in north Taiwan from shear-wave splitting, *Chin. J. Geophys.*, *54*, 627–636.
Teanby, N., J.-M. Kendall, and M. van der Baan (2004), Automation of shear-wave splitting measurements using cluster analysis, *Bull. Seismol. Soc. Am.*, *94*, 453–463.
Tillman, K. S., and T. B. Byrne (1995), Kinematic analysis of the Taiwan slate belt, *Tectonics*, *14*, 322–341, doi:10.1029/94TC02451.
Van Avendonk, H. J. A., H. Kuo-Chen, K. D. KcIntosh, L. L. Lavier, D. A. Okaya, F. T. Wu, C.-Y. Wang, C.-S. Lee, and C.-S. Liu (2014), Deep crustal structure of an arc-continent collision: Constraints from seismic travel times in central Taiwan and the Philippine Sea, *J. Geophys. Res. Solid Earth*, *119*, 8397–8416, doi:10.1002/2014JB011327.
Waldhauser, F., and W. L. Ellsworth (2000), A double-difference earthquake location algorithm: Method and application to the northern Hayward fault, California, *Bull. Seismol. Soc. Am.*, *90*, 1353–1368.
Wessel, A., M. Savage, and N. Teanby (2013), Manual for the Multiple Filter Automatic Splitting Technique (MFAST) processing codes, Version 2.0, Victoria University of Wellington.
Wessel, P., and W. H. F. Smith (1998), New, improved version of the Generic Mapping Tools released, *Eos Trans. AGU*, *79*, 579.
Wu, F. T., H. Kuo-Chen, and K. McIntosh (2014), Subsurface imaging, TAIGER experiments and tectonic models of Taiwan, *J. Asian Earth Sci.*, *90*, 173–208, doi:10.1016/j.jseaes.2014.03.024.